

Design and Placement of a Passive Clamp Snubber for Isolated SEPIC and Cuk Converters Working as Automatic Power Factor Correctors

Abraham López, Juan Rodríguez, Duberney Murillo-Yarce, Javier Sebastián and Diego G. Lamar
 University of Oviedo, Electronic Power Supply Systems Group. Campus de Viesques s/n, 33204 Gijón. Spain.
 Email: lopezantunaa.fuo@uniovi.es

Abstract — DC/DC power converters with galvanic isolation and using only one power transistor need elements that limit the voltage peaks at the beginning of the transistor turn off. These elements are called clamp snubbers. Its placement and design are well known for power converters with two reactive elements (e.g. flyback). However, different placements can be considered for those clamp snubbers in converters with higher number of reactive elements. Moreover, if the converter works as a Resistor Emulator (RE) in a Power Factor Corrector (PFC), the snubber must take into account the continuous variation of some of the electrical variables. This paper presents the study of four different placements for a passive clamp snubber network in a SEPIC converter working as an automatic RE, i.e., working in the Discontinuous Conduction Mode (DCM) and with a constant duty cycle during a line period. The value of the clamp snubber resistor needed to achieve a specific clamp voltage for these four options is determined in this paper. Moreover, the four options are compared in terms of the dissipated power in the snubber resistor. Consequently, it is possible to determine which one is going to be the best snubber option, in terms of efficiency. This study has been carried out for a SEPIC topology, and it is also valid for the Cuk one. Finally, all the study developed in this paper has been validated considering PSIM simulations and experimental results using a SEPIC prototype working as an automatic PFC.

Keywords — SEPIC converter, Clamp snubber, Power factor corrector, Resistor emulator.

I. INTRODUCTION

Galvanic isolation between input and output is very common in AC/DC and in DC/DC converters, which implies the use of several-winding magnetic components. Introducing galvanic isolation in switching-mode DC/DC converters always implies some problems due to the abrupt interruption of the current passing through the leakage inductance that the magnetic component always has. If the voltage across the transistor is clamped to a certain value by the converter topology (e.g., half-bridge and full-bridge cases), then the leakage inductance only causes parasitic oscillations. However, it can cause serious damage for the transistors in topologies such as flyback, forward, push-pull, SEPIC, Cuk, Zeta and current-feed converters, if the voltage across the transistor is not properly clamped. In these cases, it is necessary to use a snubber network [1] to limit the voltage across the transistor and to reduce the parasitic oscillations. Snubbers can be active or passive networks. Active snubbers include transistors, diodes and capacitors [1],[2]. All the energy stored in the leakage inductance is recovered when active snubbers are used, thus

avoiding losses in the snubber. However, its use increases the converter complexity and cost due to the additional transistor used, including its control and its driving circuitry. Therefore, simple passive and dissipative snubber networks are preferred for low-power and low-cost converters. A very well-known passive clamp snubber is shown in Fig.1 for a flyback converter with leakage inductance L_k . This clamp snubber is in charge of limiting the drain-source peak voltage across the transistor. In this snubber, the electric charge injected into capacitor C_c , has to be compensated with the electric charge that flows from C_c to another point in the circuit (whose voltage must be lower). The balance of these electric charges is reached for a specific voltage across C_c , which in fact is the clamp voltage. The value of the clamp snubber resistor, R_c , and its placement in the circuit determines the clamp voltage. It should be noted that the position of resistor R_c is not irrelevant, because it determines whether a part of the energy stored in C_c is returned to the input port, or, if it is completely wasted. For example, one of the R_c terminals is connected to the positive terminal of V_g in Fig.1. With this placement of R_c , current i_{Rc} flows through both R_c and V_g . Therefore, there is a partial return of energy to the input voltage source V_g . If R_c were connected in parallel with C_c

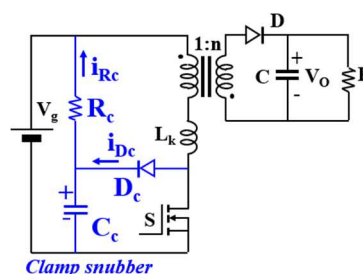


Fig. 1. Right connection of a passive clamp snubber for a flyback converter.

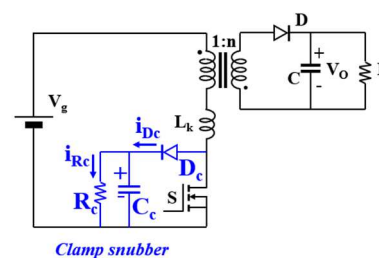


Fig. 2. Wrong connection of a passive clamp snubber for a flyback converter.

(Fig.2) this energy would not return to V_g . Therefore, the position of R_c in the circuit is not irrelevant.

A DC/DC converter can be placed between a line rectifier and a low frequency filter capacitor C_B , (as shown in Fig.3). In this case, an AC/DC converter with high power factor and low input harmonic distortion can be implemented. This is achieved by forcing the converter input current, averaged in a switching cycle, to be proportional to the converter input voltage. Once this behavior is achieved, the converter will be working as a Resistor Emulator (RE), performing a Power Factor Corrector (PFC). In the case of the converters belonging to the flyback family of converters (such as flyback, SEPIC, Cuk and Zeta converters), the easiest way to achieve RE behavior is by designing the converter as follows:

- The converter must always operate in Discontinuous Conduction Mode (DCM).
- The converter switching frequency must be constant.
- The converter duty cycle must remain almost constant during each line period [3].

The RE thus obtained is called "automatic RE" in this paper. The overall converter (line rectifier + RE) is called "automatic PFC".

Fig.3 shows a flyback converter working as an automatic PFC, with the same snubber placement as the one shown in Fig.1. However, the way to compute the value of the R_c will be different for several reasons:

- The converter input voltage, called $v_g(\phi)$ in this case, is not constant now. It changes according to line angle ϕ , because it is a rectified version of the line voltage.
- The energy stored in L_k also changes according to ϕ .
- The connection of R_c could introduce some distortion in $i_g(\phi)$, especially in the line voltage zero crossing. This effect is, in practice, negligible.

The main objective of this paper is to evaluate the clamp snubber placement for the SEPIC (Fig.4) and Cuk converters operating as automatic PFC [4]-[8]. Therefore, they must always work in DCM, operating at constant switching frequency and maintaining their duty cycle almost constant each line period. Although the study is focused on the SEPIC topology, the study carried out is also valid for the Cuk one.

This paper is organized as follows: Section II describes the SEPIC converter working as an automatic PFC. Section III

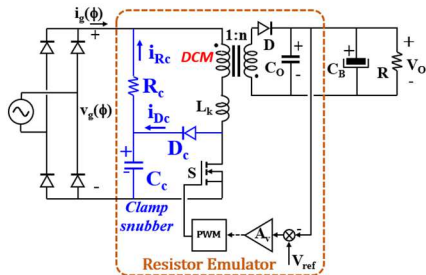


Fig.3. Flyback converter used as an automatic PFC.

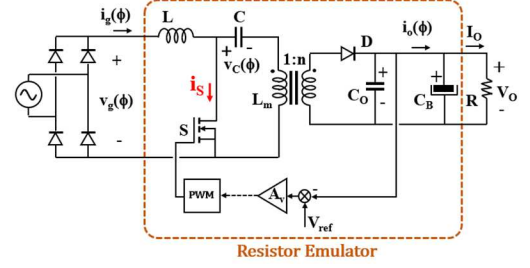


Fig.4. SEPIC converter working as an automatic PFC.

describes the four different options for a clamp snubber placement in the automatic SEPIC PFC. Simulation and experimental results are presented in Section IV. Finally, the conclusion is presented in Section V.

II. SEPIC CONVERTER WORKING AS AN AUTOMATIC PFC

Fig.4 shows a SEPIC converter working as an automatic PFC. In this converter the intermediate capacitor C is designed to have a negligible switching frequency ripple, but allowing variations of twice the line frequency [9]. Analyzing the average voltage (averaged in a switching period) in the loop made up of the rectifier output, inductance L , capacitor C and magnetizing inductance L_m , we easily obtain:

$$v_c(\phi) = v_g(\phi). \quad (1)$$

The waveform corresponding to the current passing through transistor S , i_s , is represented in Fig.5. For the sake of clarity, the switching period T_s , and the line period T_L have not been represented in the proper scale. The line-rectifier output voltage can be expressed as follows:

$$v_g(\phi) = V_g |\sin(\phi)|, \quad (2)$$

where V_g is the peak line voltage. As the converter works as an automatic PFC, the low frequency component of $i_g(\phi)$ will be:

$$i_g(\phi) = I_g |\sin(\phi)|, \quad (3)$$

where I_g is the peak value of $i_g(\phi)$. It should be noted that $i_g(\phi)$ is the average value, averaged in a switching period, of the actual current passing through inductor L . Finally, the normalized conversion ratio at the peak line voltage is:

$$M = \frac{V_o}{nV_g} \quad (4)$$

In order the SEPIC converter to achieve sinusoidal line current, the following conditions must be satisfied [9]-[11]:

- In order to avoid the Continuous Conduction Mode (CCM), the converter duty cycle must verify:

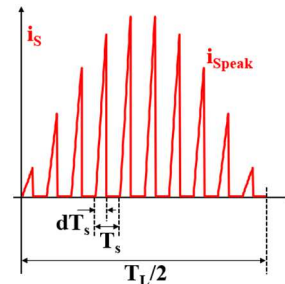


Fig.5. Transistor S current waveform.

$$d < \frac{M}{M+1}. \quad (5)$$

b) In order to avoid operation in other discontinuous conduction modes, different from the classic one, L_m :

$$L_m < ML \quad (6)$$

According to [11], the value of I_g is:

$$I_g = \frac{d^2(L + L_m)T_s}{2LL_m} V_g \quad (7)$$

A power balance in a line half-period, allows us to relate I_g , V_o and R , as follows

$$I_g = \frac{2V_o^2}{V_g R} \quad (8)$$

As capacitor C has been designed to have constant voltage during a switching period, the average value of the current passing through it during a switching period will be zero in steady state. Therefore, the average value of $i_g(\phi)$, averaged in a switching period, will be the same as the average value of $i_S(\phi)$, also averaged in the same switching period. Therefore, the peak value of the current through transistor S , $i_{Speak}(\phi)$, can be easily related to its average value, due to the triangular shape of $i_S(\phi)$:

$$i_{Speak}(\phi) = \frac{2i_g(\phi)}{d} = \frac{2I_g}{d} |\sin(\phi)| \quad (9)$$

The magnetic component that provides galvanic isolation in the converter shown in Fig.4 is a two-winding inductor, L_m being the inductance corresponding to the primary winding. The coupling between windings has been considered ideal so far. However, the actual coupling will not be ideal, resulting in the leakage inductance L_k . The presence of L_k justifies the use of a clamp snubber network in this converter.

III. PLACEMENT POSSIBILITIES FOR THE CLAMP SNUBBER IN A SEPIC-BASED AUTOMATIC PFC

Fig.6 shows the four options for the clamp snubber placement in an automatic SEPIC PFC. The main objective of the paper is to compute the power dissipated in resistor R_c for each snubber option, forcing the condition that the maximum voltage withstood by transistor S is the same in the four cases. Consequently, the option with lower value of power dissipated in R_c will be the best.

The transistor off-state voltage, without L_k , is given by:

$$v_{SOFF}(\phi) = v_C(\phi) + \frac{V_o}{n} \quad (10)$$

The maximum value of $v_{SOFF}(\phi)$ takes place at $\phi = \frac{\pi}{2}$. Considering (1), (2) and (10), we obtain:

$$v_{SOFF}\left(\frac{\pi}{2}\right) = V_g + \frac{V_o}{n} \quad (11)$$

Due to L_k , the actual transistor off-state voltage will be higher than the value given by (11). In fact, the clamp snubber is in charge of limiting this voltage to a safe value. At this point parameter λ is introduced in order to determine the increase of the voltage across transistor S when both L_k and the clamp snubber are considered. The actual transistor off-state voltage, V_{Speak} , will be now:

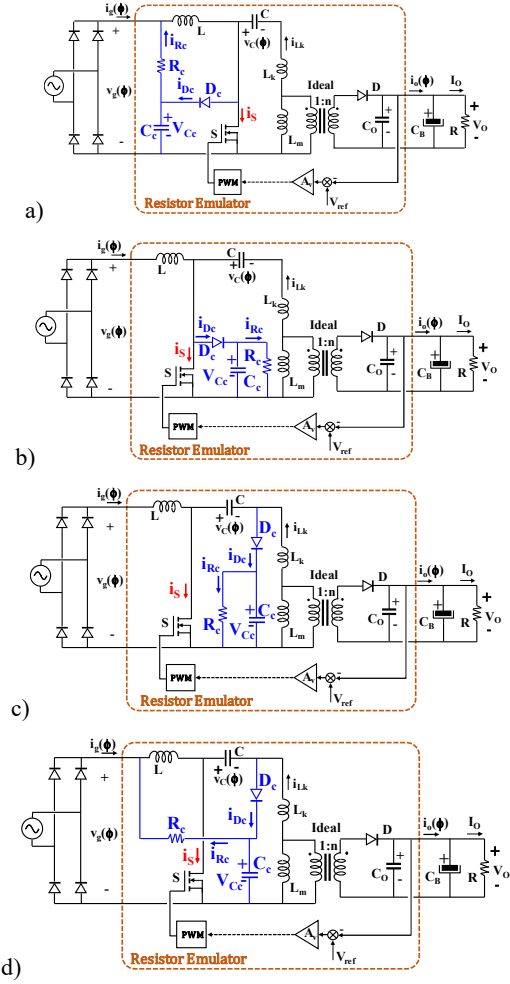


Fig.6. Different places for a clamp snubber in an automatic SEPIC PFC. a) Option A. b) Option B. c) Option C. d) Option D

$$V_{Speak} = \lambda v_{SOFF}\left(\frac{\pi}{2}\right) = \lambda(V_g + \frac{V_o}{n}) \quad (12)$$

According to (4), (12) can be rewritten as follows:

$$V_{Speak} = \lambda V_g (1 + M) \quad (13)$$

Fig.7 (a) shows an equivalent circuit to analyze the four clamp snubber options during the transistor off state. The value of voltage sources, v_1 , v_2 and v_3 are given in Table 1 for each snubber option. As this Table 1 shows, the values of these voltage sources do not change in a switching cycle.

From Fig.7(a), the waveform corresponding to current $i_{Dc}(t, \phi)$ (current passing through diode D_c after turning the transistor off) can be easily computed. As Fig.7(b) shows, the value of $i_{Dc}(t, \phi)$ coincides with $i_{Speak}(\phi)$ just in the transistor turn off (at $t = dT_s$). As D_c starts conducting in this moment, the values of V_{Speak} and V_{Cc} verifies:

$$V_{Speak} = V_{Cc} + v_2\left(\frac{\pi}{2}\right). \quad (14)$$

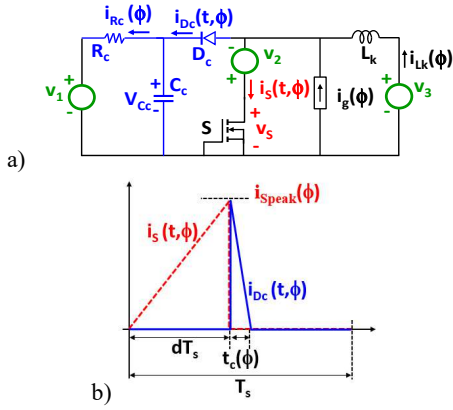


Fig.7. a) Equivalent circuit for the four snubber options during the transistor off state. b) $i_s(t, \phi)$ and $i_{Dc}(t, \phi)$ waveforms.

Table 1. Different values for v_1 , v_2 and v_3 voltage sources depending on the snubber option

	v_1	v_2	v_3
Op. A	$v_g(\phi)$	0	$v_g(\phi) + V_o/n$
Op. B	0	0	$v_g(\phi) + V_o/n$
Op. C	0	$v_g(\phi)$	V_o/n
Op. D	$v_g(\phi)$	$v_g(\phi)$	V_o/n

Taking into account the actual values of L_k , current $i_{Dc}(t, \phi)$ reaches zero in a relatively short fraction of time, called $t_c(\phi)$ in Fig.7(b). Consequently, it is assumed that current $i_g(\phi)$ does not change significantly during $t_c(\phi)$ and, therefore, can be represented by a current source in Fig.7(a). Moreover, as the values of voltage sources, v_1 , v_2 and v_3 remain constant during a switching cycle, the current waveform corresponding to $i_{Dc}(t, \phi)$ during the transistor off-state is a ramp, with a downwards slope. Obviously, diode D_c prevents a negative value for $i_{Dc}(t, \phi)$ (see Fig.7 (b)). Consequently, the value of $t_c(\phi)$ can be easily obtained from Faraday's law:

$$t_c(\phi) = \frac{L_k i_{\text{Speak}}(\phi)}{V_{Cc} - v_3}. \quad (15)$$

The average value of $i_{Dc}(t, \phi)$ in a switching period will be:

$$\langle i_{Dc}(t, \phi) \rangle_{T_s} = i_{Dc_Ts}(\phi) = \frac{L_k (i_{\text{Speak}}(\phi))^2}{2T_s (V_{Cc} - v_3)}. \quad (16)$$

Considering (9), expression (16) can be rewritten as:

$$i_{Dc_Ts}(\phi) = \frac{2L_k I_g^2 [\sin(\phi)]^2}{d^2 T_s (V_{Cc} - v_3)}. \quad (17)$$

The average value of $i_{Dc_Ts}(\phi)$ in a line half-period will be:

$$\langle i_{Dc_Ts}(\phi) \rangle_{\pi} = I_{Dc} = \frac{2L_k I_g^2}{\pi d^2 T_s} \int_0^{\pi} \frac{[\sin(\phi)]^2}{V_{Cc} - v_3} d\phi. \quad (18)$$

From Fig.7(a), the value of $i_{Rc}(\phi)$ is:

$$i_{Rc}(\phi) = \frac{V_{Cc} - v_1}{R_c}. \quad (19)$$

Its average value in a line half-period will be:

$$\langle i_{Rc}(\phi) \rangle_{\pi} = \frac{1}{\pi} \int_0^{\pi} \frac{V_{Cc} - v_1}{R_c} d\phi \quad (20)$$

In steady state, the average currents given by (18) and (20) must be equal, thus obtaining the general equation that allow us to compute the value of R_c :

$$\frac{2L_k I_g^2}{d^2 T_s} \int_0^{\pi} \frac{[\sin(\phi)]^2}{V_{Cc} - v_3} d\phi = \frac{1}{R_c} \int_0^{\pi} (V_{Cc} - v_1) d\phi. \quad (21)$$

Once value of R_c is known, the power dissipated in this resistor can be computed from the rms value of the voltage across it:

$$P_{Rc} = \frac{1}{\pi R_c} \int_0^{\pi} [(V_{Cc} - v_1)^2] d\phi. \quad (22)$$

Equations (21) and (22) are the key equations to compare the four clamp snubber options shown in Fig.6. In the following sub-section, a study of the four different clamp snubber options will be presented. It should be noted that the equivalent circuit and the waveforms of Fig.7 and the values given in Table 1 are also valid for the Cuk converter. Therefore, all the study carried out for the automatic SEPIC PFC is also valid for the Cuk case.

A. Option A of Clamp Snubber

As Table 1 shows, v_2 is zero in this case. According to (14), the value of V_{Cc} is equal to the value of V_{Speak} , given by (13). Taking into account the values of v_1 and v_3 (Table 1), (21) becomes:

$$\frac{2L_k I_g^2}{d^2 T_s V_g} H(\lambda, M) = \frac{V_g}{R_{c_A}} [\pi \lambda (1 + M) - 2], \quad (23)$$

where R_{c_A} is the value of R_c for this snubber option and $H(\lambda, M)$ is defined as follows:

$$H(\lambda, M) = \int_0^{\pi} \frac{[\sin(\phi)]^2}{\lambda(1+M) - M - |\sin(\phi)|} d\phi. \quad (24)$$

The value of R_{c_A} obtained from (23) can be rewritten as:

$$R_{c_A} = R_{\text{base}} \frac{[\lambda(1+M) - \frac{2}{\pi}] \pi}{H(\lambda, M)}, \quad (25)$$

where R_{base} is defined as:

$$R_{\text{base}} = \frac{d^2 T_s V_g^2}{2L_k I_g^2}. \quad (26)$$

According to (13) and (22), the power dissipated in R_{c_A} is:

$$P_{Rc_A} = \frac{V_g^2}{R_{c_A}} \left[\lambda^2 (1 + M)^2 + \frac{1}{2} - \frac{4}{\pi} \lambda (1 + M) \right]. \quad (27)$$

B. Option B of Clamp Snubber

In this option, v_1 and v_2 are zero. Taking into account (13) and (14), (21) becomes in this case:

$$\frac{2L_k I_g^2}{d^2 T_s V_g} H(\lambda, M) = \frac{V_g}{R_{c_B}} [\pi \lambda (1 + M)] \quad (28)$$

where R_{c_B} is the value of R_c for this option. The value of R_{c_B} obtained from (28) can be rewritten as:

$$R_{c_B} = R_{\text{base}} \frac{[\lambda(1+M)] \pi}{H(\lambda, M)}. \quad (29)$$

From (13), (14) and (22), the power dissipated in R_{c_B} is:

$$P_{Rc_B} = \frac{V_g^2}{R_{c_B}} [\lambda^2 (1 + M)^2] \quad (30)$$

C. Option C of Clamp Snubber

In this case, the values of V_{Cc} and V_{Speak} are different. Taking into account (13) and (14), the value of V_{Cc} is:

$$V_{Cc} = v_{speak} - v_g \left(\frac{\pi}{2} \right) = \lambda V_g (1 + M) - V_g. \quad (31)$$

Taking into account (31), (21) becomes:

$$\frac{2L_k I_g^2}{d^2 \tau_s} \int_0^\pi \frac{[\sin(\phi)]^2}{v_g [(\lambda-1)(1+M)]} d\phi = \frac{V_g}{R_{c,C}} \int_0^\pi [\lambda(1+M) - 1] d\phi, \quad (32)$$

where $R_{c,C}$ is the value of R_c for this option. Its value, obtained from (32), can be rewritten as:

$$R_{c,C} = R_{base} 2[\lambda(1+M) - 1](1+M)(\lambda-1). \quad (33)$$

Once $R_{c,C}$ is known, the power dissipated in this resistor can be easily computed from (22) and (31), the result being:

$$P_{R_{c,C}} = \frac{V_g^2}{R_{c,C}} (\lambda(1+M) - 1)^2. \quad (34)$$

D. Option D of Clamp Snubber

In this case, (31) also gives the value of V_{Cc} . Taking into account this value and the values of v_1 , v_2 and v_3 , (21) becomes:

$$\frac{2L_k I_g^2}{d^2 \tau_s} \int_0^\pi \frac{[\sin(\phi)]^2}{v_g [(\lambda-1)(1+M)]} d\phi = \frac{V_g}{R_{c,D}} \int_0^\pi [\lambda(1+M) - 1 - |\sin(\phi)|] d\phi, \quad (35)$$

where $R_{c,D}$ is the value of R_c for this option. Again, the value of $R_{c,D}$ obtained from (35) can be rewritten as:

$$R_{c,D} = R_{base} 2 \left[\lambda(1+M) - 1 - \frac{2}{\pi} \right] (1+M)(\lambda-1). \quad (36)$$

As in the previous cases, the power dissipated in $R_{c,D}$ can be calculated from (22) and (31), as follows:

$$P_{R_{c,D}} = \frac{V_g^2}{R_{c,D}} \left[(\lambda(1+M) - 1)^2 + \frac{1}{2} - \frac{4}{\pi} (\lambda(1+M) - 1) \right] \quad (37)$$

E. Comparison Between the Four Snubber Options

In order to compare the four snubber options, a base power value is selected as follows:

$$P_{base} = \frac{V_g^2}{R_{base}}. \quad (38)$$

This base value is used to normalize the dissipated power value corresponding to each option of clamp snubber. Therefore, (27), (30), (34) and (37) become:

$$PN_A = \frac{\lambda^2(1+M)^2 + \frac{1}{2} - \frac{4}{\pi} \lambda(1+M)}{[\lambda(1+M) - \frac{2}{\pi}] \pi} H(\lambda, M), \quad (39)$$

$$PN_B = \frac{\lambda^2(1+M)^2 + d(\frac{1}{2} + \frac{2M}{\pi})}{\lambda(1+M)\pi} H(\lambda, M), \quad (40)$$

$$PN_C = \frac{\lambda(1+M) - 1}{2(1+M)(\lambda-1)}, \quad (41)$$

$$PN_D = \frac{(\lambda(1+M) - 1)^2 + \frac{1}{2} - \frac{4}{\pi} (\lambda(1+M) - 1)}{2[\lambda(1+M) - 1 - \frac{2}{\pi}](1+M)(\lambda-1)}, \quad (42)$$

where PN_x represents the normalized power dissipated in $R_{c,x}$ when Option x has been selected as clamp snubber.

Fig.8 shows these normalized losses, for each option of clamp snubber, at different values of λ and M . As this Fig.8 shows, Option D is the one that exhibits the lowest power loss. However, for unusually low values of λ and M , Option C is the one that presents the minimum loss. By equaling (41) and (42), we can deduce the point where the power loss of these options coincide. The result is:

$$M_{C-D} = \frac{\pi+4}{4\lambda} - 1 \quad (43)$$

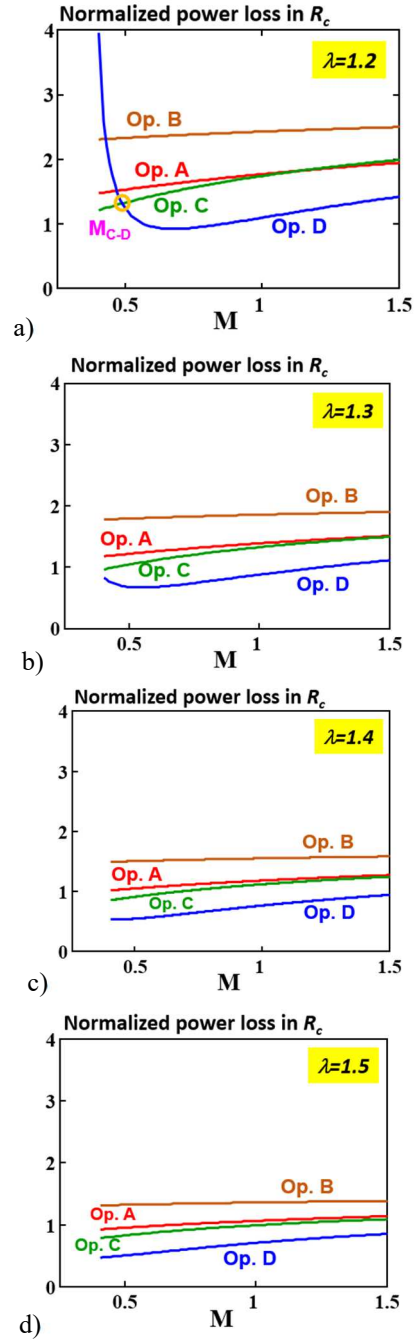


Fig.8. Normalized power loss in R_c for different values of λ and M : (a) $\lambda = 1.2$. (b) $\lambda = 1.3$. (c) $\lambda = 1.4$. (d) $\lambda = 1.5$.

Therefore, snubber power loss in Option D is lower than the corresponding loss in Option C if $M > M_{C-D}$, which is the common case. Otherwise, lower power loss is achieved in Option C. Moreover, the option that generates the highest power loss is Option B. Finally, power loss for Option A and for Option C are quite similar for all cases.

IV. EXPERIMENTAL AND SIMULATION RESULTS

In order to verify the analysis carried out to determine the value of resistor R_c and the power dissipated in this resistor for the four options of clamp snubber, an automatic SEPIC PFC has been used. First, the four clamp snubber options shown in Fig.6 have been simulated using PSIM. The values for the main SEPIC parameters are:

$$\begin{aligned} V_g &= 169.71 \text{ V} & V_o &= 48 \text{ V} & n &= 0.318 & M &= 0.89 \\ I_g &= 0.742 \text{ A} & d &= 0.413 & T_s &= 10 \text{ } \mu\text{s} & L_k &= 1.46 \text{ } \mu\text{H} \\ L &= 3.19 \text{ mH} & L_m &= 207 \text{ } \mu\text{H} & \lambda &= 1.4 \end{aligned}$$

Bearing in mind these values, the maximum voltage withstood by transistor S , without considering the voltage spike due to L_k , would be 320.7 V (11). However, a voltage spike always appears due to L_k . The clamp snubber must limit this spike to a desired value, determined by λ . Taking into consideration the value selected for λ , the actual value of the maximum voltage withstood by transistor S is 450 V (12). The converter input power, P_g , calculated from the values of V_g and I_g , is 63 W.

A prototype, similar to the simulated one, has been built. In this case, the input power is 71.3 W and the output power is 64.7 W. In order to have an output voltage of 48 V, duty cycle d was adjusted to be 0.435. The values of snubber resistors R_{c_x} , computed from (25), (29), (33) and (36), are:

$$\begin{aligned} R_{c_A} &= 107.8 \text{ k}\Omega & R_{c_B} &= 142.1 \text{ k}\Omega \\ R_{c_C} &= 75.8 \text{ k}\Omega & R_{c_D} &= 46.5 \text{ k}\Omega \end{aligned}$$

Table 2 shows a comparison between theoretical, simulation (using PSIM) and experimental results for each snubber option. These results have been obtained at the peak line voltage. The experimental values of V_{Speak} have been measured in the waveforms of Fig.9. As Table 2 shows, theoretical and simulated results fit very well, with errors lower than 7.2%. Regarding the experimental results, the values of the power loss and V_{Speak} are lower than those expected from the theoretical study. This is because the method proposed here does not consider the electric charge transferred to the transistor output capacitance, C_{oss} . A fraction of the energy variation in L_k is not transferred to capacitor C_c (and finally dissipated in R_c), but it is transferred to C_{oss} (and finally dissipated in the transistor when it turns on).

The discrepancy between theoretical and the simulated results can be predicted according to the considerations explained in [12]. Thus, total energy E_c stored in a nonlinear capacitor C_v when its voltage v changes from 0 V to a given voltage V_c can be computed as follows:

$$E_c = \int_0^{V_c} v \cdot C_v dv. \quad (44)$$

The transistor used in the converter prototype was a STP18N60DM2. Fig.10 shows the C_{oss} - V_{ds} curve for this transistor, obtained from its datasheet. From the information given in this Fig.10, the value of the energy stored in C_{oss} can be estimated according to (44). Thus, a numerical approach to (44) from 0 V to 400 V gives that the energy stored in C_{oss} is 2.974 μ J. This energy is wasted in the transistor during the transistor turn on, instead of being transferred to C_c . As the switching period is 10 μ s, this energy means a power dissipation of 0.2974 W. This power dissipation must be discounted from the power transferred to C_c and finally dissipated in R_c . Therefore, the actual value of V_{Cc} (and, consequently, of V_{Speak})

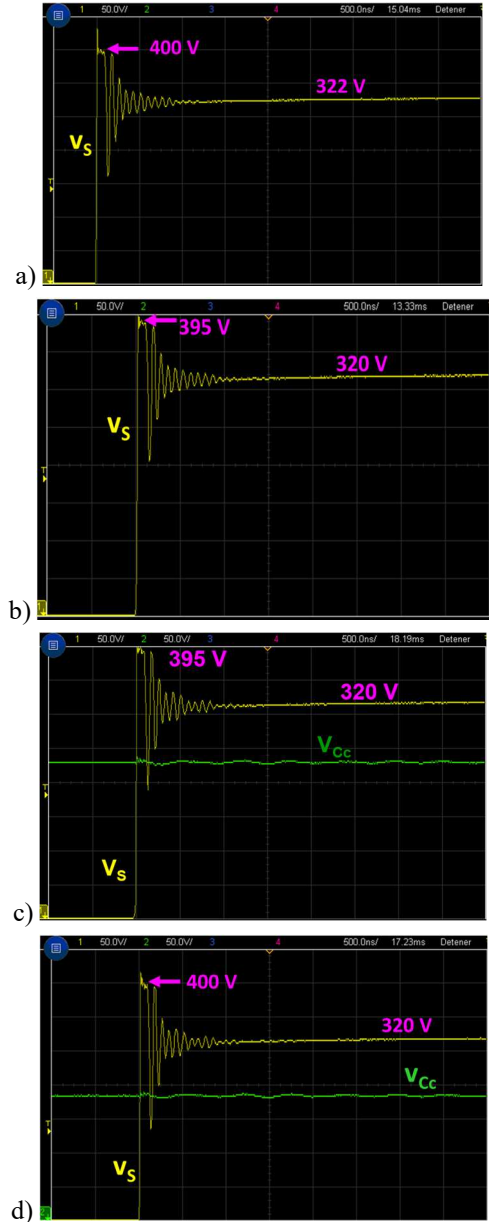


Fig.9. Experimental waveforms corresponding to the transistor drain-source voltage at the peak of the line voltage: a) Option A, b) Option B, c) Option C, and d) Option D.

Table 2. Comparison between theoretical, simulated and measured values for the four snubber options.

	A	B	C	D
Theoretical loss (W)	1.104	1.421	1.03	0.69
Simulated loss (W)	0.956	1.347	0.93	0.63
Measured loss (W)	0.634	1.10	0.749	0.411
V_{Speak} simulated (V)	425.20	423.30	426.80	429.10
V_{Speak} measured (V)	400	395	395	400

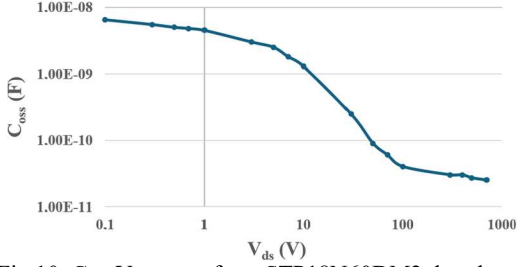


Fig.10. C_{oss} - V_{ds} curve from STP18N60DM2 datasheet.

and of P_{Rc} will be clearly lower than the one computed in the theoretical analysis.

To quantify this effect, parameter α is defined as follows:

$$\alpha = \frac{P_{Rc} - P_{Coss}}{P_{Rc}} \quad (45)$$

where P_{Coss} is the power transferred to C_{oss} . The actual power dissipated in R_c taking into consideration P_{Coss} is called P_{Rc}^* . Its value is:

$$P_{Rc}^* = P_{Rc} - P_{Coss} = \alpha P_{Rc}. \quad (46)$$

It should be noted that P_{Rc}^* is always lower than P_{Rc} . As R_c has been calculated without taking into account P_{Coss} , the actual value of V_{Cc} , V_{Cc}^* , will also be lower than V_{Cc} . According to (14), the actual value of V_{Speak} , V_{Speak}^* , will be:

$$V_{Speak}^* = V_{Cc}^* + v_2. \quad (47)$$

From V_{Speak}^* , a new parameter λ^* can be defined as follows:

$$\lambda^* = \frac{V_{Speak}^*}{V_g(1+M)}. \quad (48)$$

The procedure to compute V_{Speak}^* (and, therefore, λ^*) is based on adapting (22) to the fact that the actual power dissipated in R_c is P_{Rc}^* , instead of P_{Rc} . Thus, (22) becomes:

$$P_{Rc}^* = \alpha P_{Rc} = \frac{1}{\pi R_c} \int_0^\pi [(V_{Cc}^* - v_1)^2] d\phi. \quad (49)$$

This equation allows us to obtain the value of V_{Cc}^* for a given value of α (and, therefore, of P_{Coss}). Once V_{Cc}^* is known, (47) and (48) give us the values of V_{Speak}^* and λ^* .

The results obtained for the four options of clamp snubber applying this procedure are shown below. In all cases, λ_x^* and α_x are the values of λ^* and α for snubber option x. The results obtained are the following:

A. Option A:

Taking into account (27), (49) becomes:

$$\alpha_A \left[\lambda^2(1+M)^2 + \frac{1}{2} - \frac{4}{\pi} \lambda(1+M) \right] = \lambda_A^{*2}(1+M)^2 + \frac{1}{2} - \frac{4}{\pi} \lambda_A^*(1+M). \quad (50)$$

Solving this equation, we obtain:

$$\lambda_A^* = \frac{-b_A + \sqrt{b_A^2 - 4a_A c_A}}{2a_A} \quad (51)$$

where:

$$a_A = (1+M)^2 \quad (52)$$

$$b_A = -\frac{4}{\pi}(1+M) \quad (53)$$

$$c_A = \frac{1}{2} - \alpha_A \left[\lambda^2(1+M)^2 + \frac{1}{2} - \frac{4}{\pi} \lambda(1+M) \right] \quad (54)$$

In the prototype, $P_{Rc_A} = 1.104$ W and $P_{Coss} \approx 0.3$ W. According to (45), $\alpha_A = 0.728$. From (51), $\lambda_A^* = 1.24$.

B. Option B:

Taking into account (30), (49) becomes:

$$\alpha_B \lambda^2(1+M)^2 = \lambda_B^{*2}(1+M)^2. \quad (55)$$

This equation can be easily solved. The result is:

$$\lambda_B^* = \lambda \cdot \sqrt{\alpha_B}. \quad (56)$$

In the prototype, $P_{Rc_B} = 1.421$ W. Therefore, $\alpha_B = 0.789$. From (56), we obtain $\lambda_B^* = 1.243$.

C. Option C:

From (34), (49) becomes:

$$\alpha_C \cdot [\lambda(1+M) - 1]^2 = [\lambda_C^*(1+M) - 1]^2. \quad (57)$$

The solution of (57) is:

$$\lambda_C^* = \frac{\sqrt{\alpha_C} \cdot [\lambda(1+M) - 1] + 1}{M+1}. \quad (58)$$

In the prototype, $P_{Rc_C} = 1.03$ W. Hence, $\alpha_C = 0.709$. Using (58), we obtain $\lambda_C^* = 1.262$.

D. Option D:

Using (37), (49) leads to:

$$\begin{aligned} \alpha_D \left[(\lambda(1+M) - 1)^2 + \frac{1}{2} - \frac{4}{\pi} (\lambda(1+M) - 1) \right] \\ = (\lambda_D^*(1+M) - 1)^2 + \frac{1}{2} \\ - \frac{4}{\pi} (\lambda_D^*(1+M) - 1). \end{aligned} \quad (59)$$

Solving (59), we obtain:

$$\lambda_D^* = \frac{-b_D + \sqrt{b_D^2 - 4a_D c_D}}{2a_D}, \quad (60)$$

where:

$$a_D = (1+M)^2, \quad (61)$$

$$b_D = -\left(\frac{4}{\pi} + 2\right)(1+M), \quad (62)$$

$$\begin{aligned} c_D = \frac{3}{2} + \frac{4}{\pi} - \alpha_D \left[[\lambda(1+M) - 1]^2 + \frac{1}{2} \right. \\ \left. - \frac{4}{\pi} [\lambda(1+M) - 1] \right]. \end{aligned} \quad (63)$$

In the prototype, $P_{Rc_D} = 0.69$ W. Therefore, $\alpha_D = 0.565$. From (60), we obtain $\lambda_D^* = 1.253$.

Table 3 shows a comparison between the value of V_{Speak} measured and V_{Speak}^* for the four snubber options. The values of V_{Speak}^* have been obtained from the values of λ_x^* already obtained and (48). As this Table 3 shows, excellent agreement between the results measured in the waveforms of Fig.9 and those predicted after taking into account P_{Coss} (the power transferred to C_{oss}) has been finally achieved.

Table 3. Comparison between P_{Rc}^* losses, V_{Speak} measured and V_{Speak}^* values for the four snubber options.

	A	B	C	D
V_{Speak} measured (V)	400	395	395	400
V_{Speak}^* (V)	397.78	398.82	404.86	401.86
P_{Rc}^* (W)	0.804	1.121	0.730	0.389

In some of the waveforms of Fig.9, some additional voltage spikes can be observed over the value marked for V_{Speak} . Thus, the spike shown in Fig.9(a) achieves about 420 V. These spikes are due to the parasitic inductance and resistance of diode D_c , capacitor C_c and the connection between these elements and the transistor. In the case of options C and D, the parasitic elements of capacitor C must be taken into consideration too. Obviously, a proper selection of the snubber devices and a proper design of the converter PCB is of primary concern. Fortunately, these additional spikes are quite narrow and do not exceed transistor voltage rating.

Finally, the fact of existing more options for the placement of the clamp snubber in the case of the SEPIC PFC represents a practical advantage of this topology over the use of the flyback PFC for the same application. In the case of the flyback PFC, an input filter made up of an inductor and a couple of capacitors must be placed at the flyback input to alleviate the differential-mode noise without deteriorating the power factor (see Fig.11). Therefore, the actual number of power elements (semiconductors and reactive elements) is similar in the case of both the flyback and the SEPIC PFC (see Fig.12). However, the SEPIC PFC has more options for the clamp snubber than the flyback PFC due to capacitor C. As demonstrated in this paper, lower power will be dissipated in snubber resistor R_c if Option D is selected. This option is not possible in the flyback topology.

V. CONCLUSIONS

The placement of a passive clamp snubber in isolated SEPIC and Cuk converters working as automatic PFC is not irrelevant. This work presents four different options for the placement of a passive clamp snubber, analyzing the value of snubber resistor R_c and of the power dissipated in this resistor for the four cases. The theoretical analysis has been normalized by selecting proper base values for resistance and power. According to the normalized values of the power loss in R_c , the option that exhibits the lowest power loss is option D, at least for common design values of λ and M . On the contrary, option B is the one that exhibits the highest power loss. Options A and C present similar values of power loss, higher than Option D, but lower than Option B. The conclusions of this study have been validated by simulation and with experimental results. The results obtained by simulation agree very well the theoretical study. Regarding the experimental results obtained for the maximum voltage across the transistor and the power dissipated in the snubber resistor, they are lower than the predicted by the study. However, this discrepancy can be overcome by taking into account the power transferred to the transistor output capacitance (C_{oss}). Once this power is discounted from the power dissipated in R_c , excellent agreement is observed between the new predicted results and the experimental results.

ACKNOWLEDGMENTS

This work has been carried out by funding from the Asturias government through the SV-PA-21-AYUD/2021/51931 project, and from the Spanish government through the PID2022-136969OB-I00, PID2021-127707OB-C21, MCINN-22-TED2021-130939B-I00 and MCINN-23-PID2022-136969OB-I00 projects.

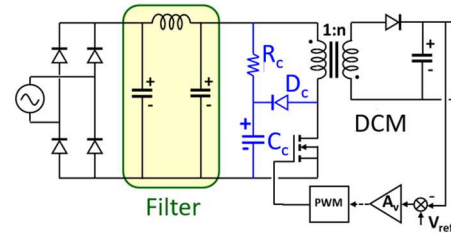


Fig.11. Flyback PFC with the best clamp snubber option.

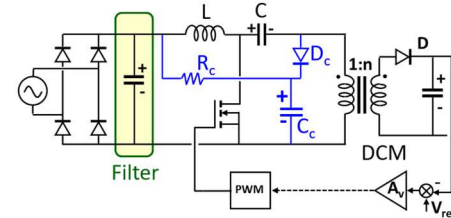


Fig.12. SEPIC PFC with the best clamp snubber option.

REFERENCES

- [1] P.C. Todd, "Snubber circuits: Theory, design and application". Unitrode Power Supply Design Seminar, 1993, pp. 2.1-2.17.
- [2] B. Carsten. "Design techniques for transformer active reset circuits at high frequencies and power levels". High Frequency Power Conversion (HFPC) Conference, 1990, pp. 235-246.
- [3] R. Erickson, M. Madigan, and S. Singer, "Design of a simple high power-factor rectifier based on the flyback converter", in Fifth Annual Proceedings on Applied Power Electronics Conference and Exposition, 1990, pp. 792-801.
- [4] J. Sebastián, J. Uceda, J. A. Cobos, J. Arau, and F. Aldana, "Improving power factor correction in distributed power supply systems using pwm and ZCS-QR Sepic topologies", in PESC '91 Record 22nd Annual IEEE Power Electronics Specialists Conference, 1991, pp. 780-791.
- [5] M. Mahdavi and H. Farzanehfar, "Bridgeless SEPIC PFC rectifier with reduced components and conduction losses", IEEE Trans. Ind. Electron., vol. 58, Sep. 2011.
- [6] E. H. Ismail, "Bridgeless SEPIC rectifier with unity power factor and reduced conduction losses", IEEE Trans. Ind. Electron., vol. 56, pp. 1147-1157, Apr. 2009.
- [7] A. J. Sabzali, E. H. Ismail, M. A. Al-Saffar, and A. A. Fardoun, "New bridgeless DCM Sepic and Cuk PFC rectifiers with low conduction and switching losses", IEEE Trans. Ind. Appl., vol. 47, no. 2, pp. 873-881, Mar./Apr. 2011.
- [8] P. J. S. Costa, C. H. I. Font, and T. B. Lazzarin, "A family of single-phase voltage-doubler high-power-factor SEPIC rectifiers operating in DCM", IEEE Trans. Power Electron., vol. 32, no. 6, pp. 4279-4290, Jun. 2017.
- [9] D. S. L. Simonetti, J. Sebastián and J. Uceda. "The discontinuous conduction mode SEPIC and Ćuk power factor pre-regulators: Analysis and design". IEEE Trans. on Industrial Electronics, vol. 44, n° 5, 1997, pp. 630-637
- [10] J. Sebastián, J. A. Cobos, J. M. Lopera and J. Uceda. "The determination of the boundaries between continuous and discontinuous conduction modes in PWM dc-to-dc converters used as power factor preregulators". IEEE Trans. on Power Electronics, vol.10, n° 5, 1995, pp. 574-582.
- [11] D. Murillo-Yarce, J. Rodriguez, F. Loose, M. Hernando and J. Sebastian, "Study of SEPIC and Ćuk converters working as automatic Power Factor Corrector when operating in unusual discontinuous conduction modes," 2024 IEEE Applied Power Electronics Conference and Exposition (APEC), Long Beach, CA, USA, 2024, pp. 42-49.
- [12] D. Costinett, D. Maksimovic and R. Zane, "Circuit-oriented treatment of nonlinear capacitances in switched-mode power supplies". IEEE Trans. on Power Electronics, vol.30, n° 2, 2015, pp. 985-995.